Available online at www.eccomasproceedia.org
Eccomas Proceedia COMPDYN (2021) 5028-5038

ECCOMAS
Proceedia

COMPDYN 2021
8th ECCOMAS Thematic Conference on
Computational Methods in Structural Dynamics and Earthquake Engineering
M. Papadrakakis, M. Fragiadakis (eds.)
Streamed from Athens, Greece, 28 - 30 June 2021

FREE VIBRATION RESPONSE OF LONG MULTI-SPAN BRIDGES ACCOUNTING FOR SOIL-STRUCTURE INTERACTION

Pieter Reumers, Geert Lombaert, and Geert Degrande

KU Leuven, Department of Civil Engineering, Structural Mechanics Section
Kasteelpark 40, 3001 Leuven, Belgium
e-mail: {pieter.reumers,geert.lombaert,geert.degrande}@kuleuven.be

Abstract. *This paper investigates the effect of soil-structure interaction (SSI) on the free vibration response of long multi-span bridges. A numerical case study of a continuous concrete box girder bridge is presented. For several bridge lengths, the influence of SSI on modal characteristics is studied. Furthermore, if the bridge is assumed to be infinitely long, periodic structure theory is used to compute the dispersion curves of the non-decaying waves that propagate through the bridge. The stop- and passbands are related to the natural frequencies of the bridges with finite length.*

Keywords: multi-span bridges, soil-structure interaction, modal analysis, piled foundation, periodic structure theory

ISSN:2623-3347
Peer-review under responsibility of the organizing committee of COMPDYN 2021.
doi: 10.7712/120121.8847.18976

1 INTRODUCTION

Road and railway bridges are frequently constructed in regions with changing topography or soft sub-soil conditions, and in dense urban areas due to space limitations. Often, these bridges consist of identical spans repeated over a long distance resulting in a convenient and cost-effective design. This paper investigates the effect of soil-structure interaction (SSI) on their free vibration response, which is important as the structure's modal characteristics (mode shapes, natural frequencies, modal damping ratios) are commonly used in structural health monitoring.

The influence of SSI on the modal characteristics of long multi-span bridges is often neglected in finite element model updating procedures [1, 2], as this significantly reduces the model complexity and is typically a valid simplification when the structure is founded on stiff soil. However, for short (single-span) bridges, many studies have highlighted the importance of SSI on modal characteristics. Romero et al. [3] studied the dynamic response of single-span, simply supported railway bridges under moving loads. They conclude that the resonant train speed is lower when dynamic SSI is accounted for, due to the lower natural frequency of the bridge. Furthermore, they report a substantial increase of the modal damping ratio if the soil stiffness is low, resulting in lower bridge deck acceleration at mid-span. Östlund et al. [4] investigate the effect of different foundation types and span lengths on the response and modal characteristics of a single-span railway bridge. They show that the modal damping ratio increases for shorter span lengths and that the bridge deck acceleration is generally higher in the case of fixed supports.

In this paper, a case study of a continuous concrete box girder bridge is presented in order to analyze the influence of SSI on the modal characteristics of long, repetitive bridges. Three cases are considered for the soil stiffness: a soft, medium, and stiff soil. Furthermore, the analysis is performed for a bridge with 5 spans, 15 spans, and an infinitely long bridge.

The paper is organized as follows. Section 2 introduces the numerical case study. Section 3 focuses on the influence of SSI and bridge length on the free vibration response of the bridge; the influence on modal characteristics is studied for the bridges with finite length, which are subsequently linked to dispersion curves of free waves propagating through the infinitely long bridge. Section 4 concludes the paper.

2 NUMERICAL CASE STUDY

This section presents a numerical case study of a continuous concrete box girder bridge founded on piled foundations. In the past decades, a large number of such bridges have been built in many European countries [5]. The advantage over simply supported box girder bridges, which remain the standard in China, is their greater slenderness (ranging between 12 and 14) and generally lower dynamic response. The geometry and material properties are based on a literature survey of existing box girder bridges presented by Kang et al. [5], Yan et al. [6], and Cascales Fernández et al. [7].

2.1 Bridge geometry

Figure 1a shows a single span of the railway bridge. The span length L equals 24 m. The bridge cross section is a concrete box girder with uniform height (Figure 1b). The bridge deck is periodically supported by 6 m high piers with a rectangular cross section of 5.5 m by 1 m. At each pier, the bridge deck rests on two bearings. The concrete has a Young's modulus $E = 30$ GPa, a Poisson's ratio $\nu = 0.25$, and a density $\rho = 2500$ kg/m^3. Rate-independent hysteretic material damping in the frequency domain is modeled by introducing a complex

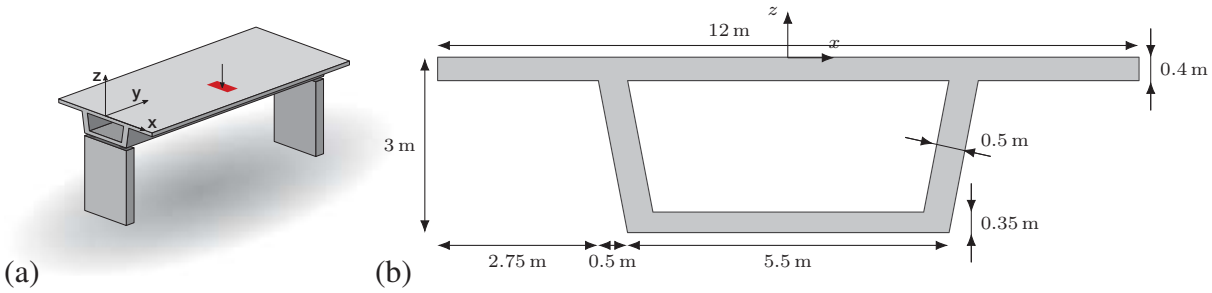

Figure 1: (a) Single bridge span and (b) cross section of the bridge deck. The red area indicates the area to which the load is applied.

Young's modulus $E^* = E(1 + 2\mathrm{i}\beta)$, where a material damping ratio β of 0.02 is assumed.

The deck and piers are both modeled with 8-node quadratic shell elements based on Reissner-Mindlin plate theory. Figure 2 shows the FE model of the pier and bridge deck. The maximum element size equals 1 m for the deck and 0.5 m for the pier. Each bearing is represented by constraint equations between two nodes on the deck and two corresponding nodes on the pier. For the left bearing (in red), the vertical as well as the lateral displacement of the deck and pier are coupled. For the right bearing (in blue), only the vertical displacement is coupled. In the longitudinal direction, the displacement of the deck and pier is only coupled at one of the bridge piers.

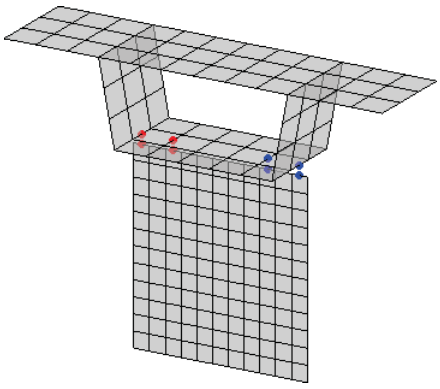

Figure 2: Finite element model of a pier and part of the bridge deck. At the nodes representing the left bearing (in red), vertical and lateral displacements are coupled using constraint equations, while at the right bearing (in blue), only vertical displacements are coupled.

2.2 Bridge length

Three bridges are considered in this paper: a bridge with 5 spans, a bridge with 15 spans, and an infinitely long bridge. For the first two cases, the length of the end spans equals half the regular span length. At both bridge ends, constraint equations (as explained in Subsection 2.1) are used to account for the support conditions: the vertical displacements are prohibited by both supports, while lateral displacements are prohibited by the left support.

2.3 Piled foundation

Each pier is supported by a piled foundation that consists of eight piles connected to a pile cap with a thickness of 1 m. The pile cap is assumed to be rigid, as is the connection between the pier and the pile cap, and the pile cap and the piles. Figure 3b shows the geometry of the

piled foundation. The piles have a diameter of 0.4 m and a length of 10 m. The piles and pile cap are made of concrete with Young's modulus $E = 35$ GPa, Poisson's ratio $\nu = 0.25$, and density $\rho = 2500$ kg/m^3. No material damping is considered for the piled foundation.

Each piled foundation is embedded in a horizontally layered soil (Figure 3a) consisting of a 9 m thick top layer on top of a halfspace. Three cases are considered for the top layer: a soft soil, a medium soil, and a stiff soil. The underlying halfspace consists of stiff soil. Hence, the stiff soil case corresponds to a homogeneous halfspace. The dynamic soil characteristics are specified in Table 1. The piles reach 1 m into the stiff halfspace.

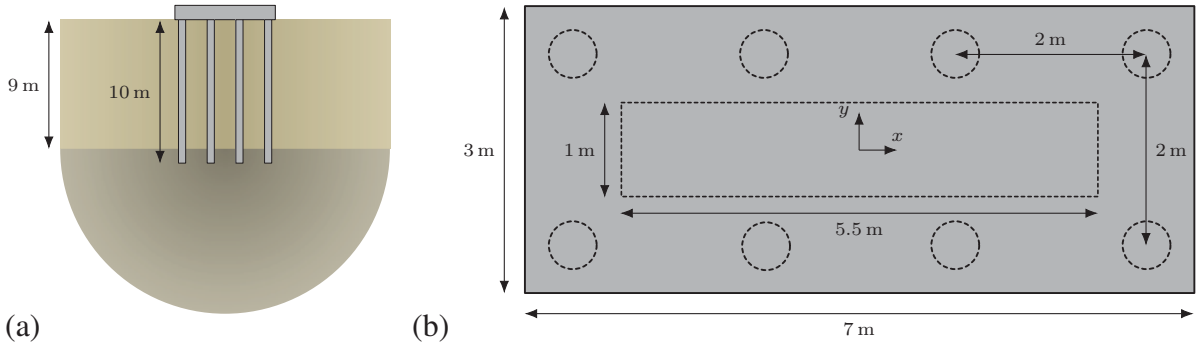

Figure 3: (a) Piled foundation embedded in a horizontally layered halfspace and (b) geometry of the piled foundation.

Soil type	C_s [m/s]	C_p [m/s]	ρ [kg/m^3]	β_s [-]	β_p [-]
Soft soil	100	200	1800	0.02	0.02
Medium soil	200	400	1800	0.02	0.02
Stiff soil	300	600	1800	0.02	0.02

Table 1: Dynamic soil characteristics: shear wave velocity C_s, dilatational wave velocity C_p, density ρ, and material damping ratio's β_s and β_p in shear and dilatational deformation.

The soil and the piles are both modeled with 10-node quadratic tetrahedral elements. A perfectly matched layer (PML) is used to absorb waves at the edges of the FE model [8, 9]. The element size l_e is chosen such that the distance between two nodes is always less than one-eight of a shear wavelength for each frequency, both in the physical soil domain and the PML. The width of the physical soil domain between the PML and the foundation is chosen as one half shear wavelength at 50 Hz .

The FE-PML formulation used in this work is described in detail by Papadopoulos et al. [10], and based on the work of Chew and Qiu [8] and Basu and Chopra [9]. As explained in [10], the PML stretch functions consist of third-degree polynomial functions with $\alpha_0 = \pi C_\mathrm{s}/(l_\mathrm{e}\omega) - 1$ and $\alpha_1 = 20C_\mathrm{s}$, controlling the attenuation of evanescent and propagating waves inside the PML domain, respectively. The FE-PML model of the piled foundation is validated using a finite element-boundary element model (FE-BE) model.

The dynamic stiffness of the piled foundation is defined as the forces or moments required to impose a unit displacement or rotation of the rigid pile cap. The real part determines the stiffness, while the imaginary part depends on the material and radiation damping in the soil.

Figure 4 shows the stiffness and damping coefficients of a single piled foundation modeled with a 3D FE-PML model and a 3D FE-BE model. The pile cap is assumed to be rigid and

massless. Figure 4a shows the vertical stiffness $\mathrm{Re}(k_{zz})$ of the piled foundation embedded in soft, medium, and stiff soil. The static stiffness increases with increasing soil stiffness. An increase in stiffness is observed for the soft soil around 22 Hz due to interaction between the individual piles. When the shear wavelength in the soil equals twice the pile spacing, the piles vibrate in anti-phase motion leading to a stiffer behavior of the piled foundation [11]. The pile-soil-pile interaction effect is observed around 45 Hz for the medium soil. For the stiff soil, a peak in the stiffness function is expected around 75 Hz. Figure 4b shows the vertical damping $\mathrm{Im}(k_{zz})$. In the low frequency range it is observed that, as the soil stiffness of the top layer decreases, the damping decreases as well. This is explained by the fact that, for a soft layer on a stiffer halfspace, wave propagation in the soft top layer only occurs at frequencies above the cut-on frequency, activating radiation damping. This effect is more pronounced as the relative difference in stiffness between the top layer and the halfspace increases. Furthermore, the peaks due to pile-soil-pile interaction are also observed in the damping curves.

Figure 4c shows the rocking stiffness $\mathrm{Re}(k_{\varphi_x\varphi_x})$ around the x-axis, which is significantly lower than the rocking stiffness $\mathrm{Re}(k_{\varphi_y\varphi_y})$ around the y-axis shown in Figure 4e, due to the smaller eccentricity of the piles with respect to the center. Again, the effect of pile-soil-pile interaction is observed as peaks in the stiffness functions. Figures Figure 4d and Figure 4f show the corresponding damping values $\mathrm{Im}(k_{\varphi_x\varphi_x})$ and $\mathrm{Im}(k_{\varphi_y\varphi_y})$ for the rocking motion of the piled foundation around the x- and y-axis, respectively. Finally, the results obtained with the 3D FE-PML and 3D FE-BE model are in very good agreement across the entire frequency range. The slight discrepancy in the high frequency range is attributed to the FE discretization.

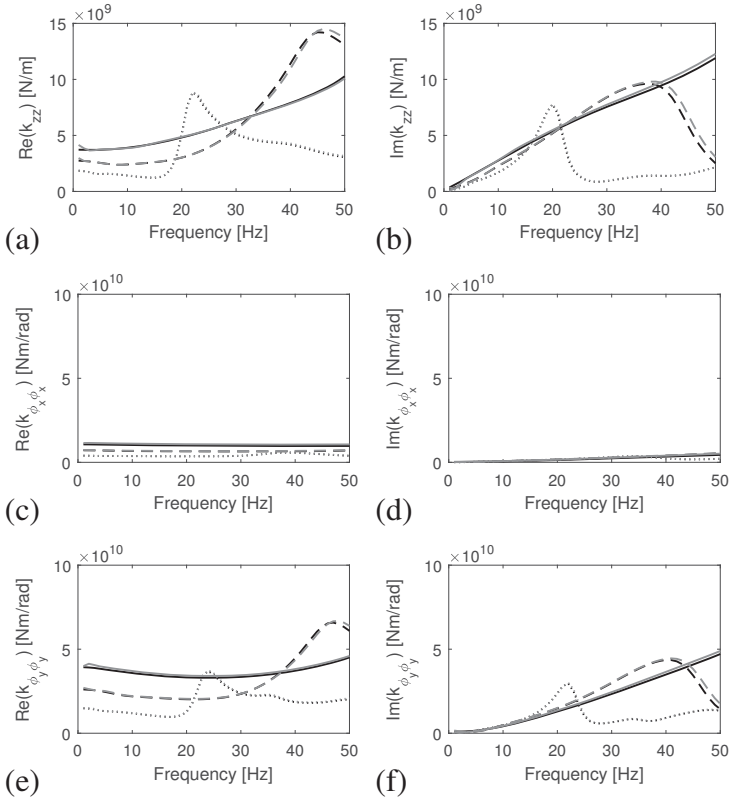

Figure 4: Vertical (a) stiffness $\mathrm{Re}(k_{zz})$ and (b) damping $\mathrm{Im}(k_{zz})$, rocking (c) stiffness $\mathrm{Re}(k_{\varphi_x\varphi_x})$ and (d) damping $\mathrm{Im}(k_{\varphi_x\varphi_x})$, and rocking (e) stiffness $\mathrm{Re}(k_{\varphi_y\varphi_y})$ and (f) damping $\mathrm{Im}(k_{\varphi_y\varphi_y})$ for the piled foundation embedded in stiff (solid line), medium (dashed line), and soft soil (dotted line). The black and gray lines correspond to the results obtained with the FE-BE and FE-PML model, respectively.

3 FREE VIBRATION RESPONSE

The effect of SSI and bridge length (number of spans) on the natural frequencies and mode shapes is investigated. Furthermore, the dispersion curves of the non-decaying waves propagating through an infinitely long bridge are computed and related to the modal characteristics of the bridges with finite length.

3.1 Modal characteristics

A 3D FE model of the bridge with 5 spans (Figure 5) is constructed in order to compute its modal characteristics. First, SSI is neglected and the piers are assumed fixed at the bottom. Figure 6a shows the first five mode shapes and corresponding natural frequencies of the bridge.

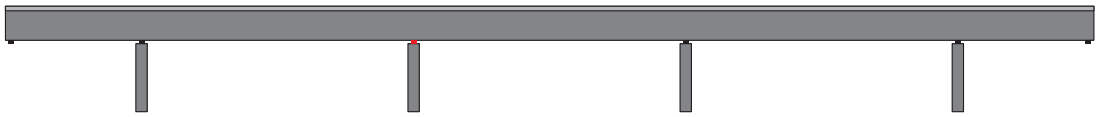

Figure 5: Bridge with 5 spans. The support where longitudinal displacement of the bridge deck and pier are coupled is shown in red.

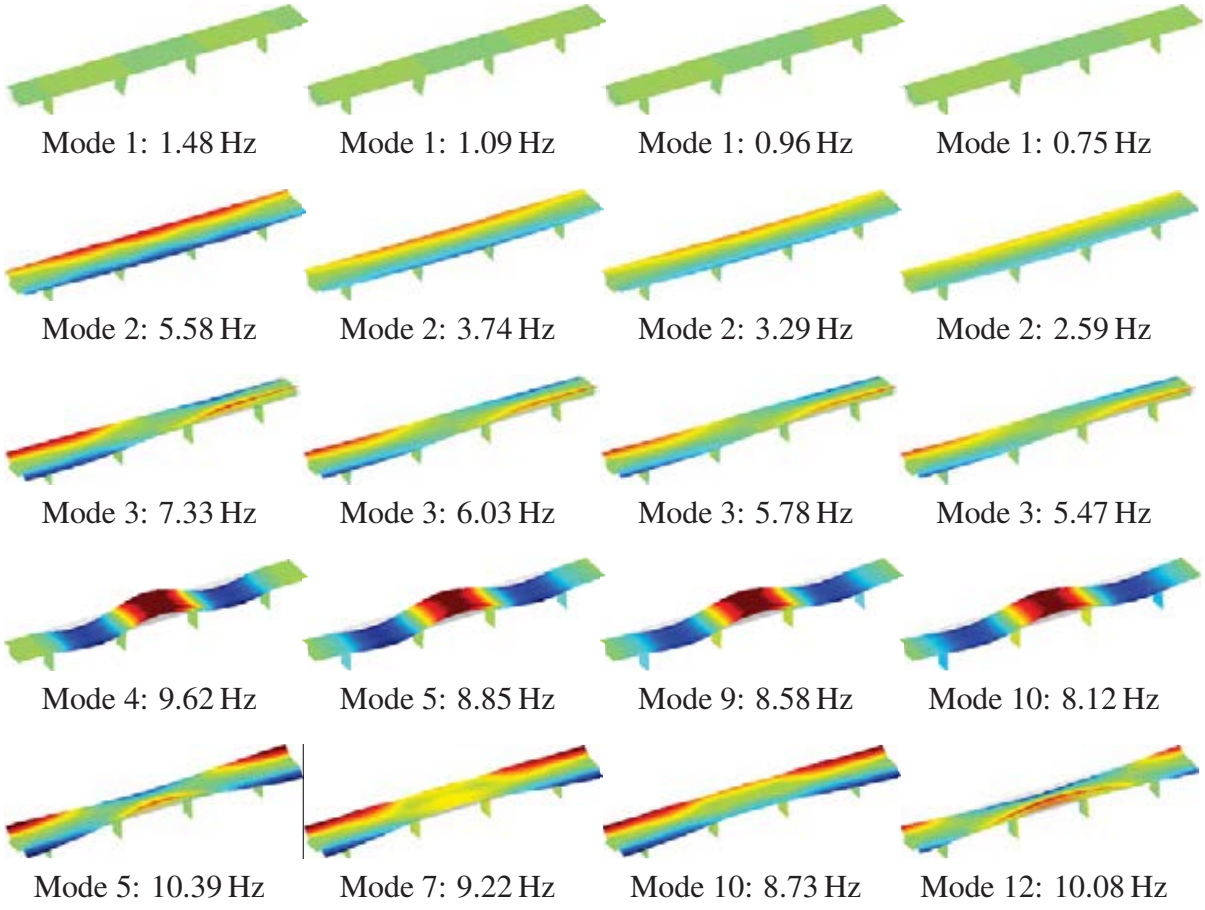

Figure 6: Mode shapes and natural frequencies of the bridge with 5 spans computed for (a) the case without SSI, (b) the stiff soil, (c) the medium soil, and (d) the soft soil. The color scheme indicates the magnitude of the vertical displacement while the undeformed structure is shown in light gray.

The first mode is a longitudinal translation mode of the bridge deck, which is not excited by a vertical load acting on the bridge. The top of the second pier translates with the bridge deck due to the fixed coupling at this support. Modes 2, 3, and 5 are torsional modes for which the dominant vertical displacement is situated in the flanges of the box girder. Mode 4 is a vertical bending modes of the bridge for which neighboring spans oscillate out-of-phase.

3.1.1 Influence of SSI

In order to assess the effect of SSI on the modal characteristics, the static foundation stiffness is added to each bridge pier (using springs) and the modal characteristics are recomputed. Alternatively, the dynamic stiffness at a resonance frequency of the bridge without SSI could be used [12]. Note that, in the present case, the dynamic stiffness does almost not depend on the frequency between 0 and 15 Hz (Figure 4), where the first bridge modes are situated, so that the outcome would be very similar.

In order to properly match the mode shapes and corresponding natural frequencies of the bridge with and without SSI, the Modal Assurance Criterion [13] is used. Whenever mode numbers are mentioned in the following, we refer to the modes without SSI. Figure 7a shows the MAC values computed for the first 20 mode shapes without SSI and with the stiff soil. The first 13 modes can be matched reasonably well to the mode shapes of the bridge without SSI. The order of the modes, however, changes when SSI is accounted for. In modes 8 to 10 (with SSI), the piers rotate around the x-axis and the bridge deck remains still as the piers can rotate freely with respect to the bridge deck. Figure 7b shows the MAC values computed for the medium soil. In this case, only the first five mode shapes can be matched accurately to the modes without SSI. For the soft soil case in Figure 7c, it is observed that only the first three modes are matched relatively well to the modes computed without SSI. Modes 4 to 6 (with SSI) are local rotation modes of the piers, which correspond to lower natural frequencies compared to the case with stiff soil. Mode 4, the first vertical bending mode, now corresponds to mode 7 with SSI.

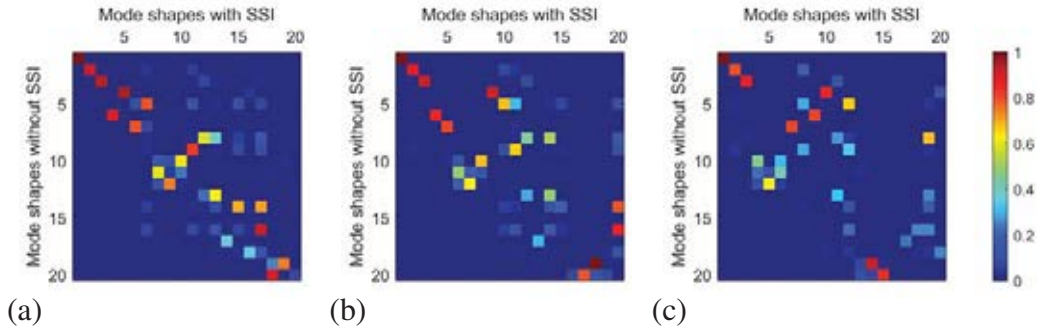

Figure 7: MAC values between the mode shapes computed without and with SSI for the case of (a) stiff soil, (b) medium soil, and (c) soft soil.

Using the MAC values presented in Figure 7, the mode shapes of the bridge with and without SSI are matched. The mode shapes computed with the stiff soil are shown in Figure 6b. Overall, the mode shapes are very similar to those without SSI. For the torsional modes, rocking motion of the piers around the y-axis is observed due to the flexibility of the soil, resulting in significantly lower natural frequencies. Figure 6c shows the mode shapes computed with the medium soil. The natural frequencies are lower compared to those computed with the stiff soil, but the

mode shapes are very similar. Figure 6d shows the mode shapes computed with the soft soil. Compared to the case without SSI, a reduction of 53 % and 25.4 % on the natural frequency of the first and second torsional mode is predicted. The reduction of the natural frequency for the first vertical bending mode is 15.6 %. For mode 5, almost no decrease in natural frequency is observed, but the MAC value shows a poor agreement with the corresponding mode shape without SSI.

It can be concluded that, as the soil stiffness decreases, the effect of SSI on the modal characteristics of the bridge increases. Torsional modes in particular are significantly affected by SSI. Hence, when predicting the forced vibration response or performing structural health monitoring of multi-span bridges, it is important to account for SSI especially when soft soil conditions prevail.

3.1.2 Influence of the bridge length

Next, the influence of the bridge length (number of spans) on the natural frequencies is investigated. For periodic structures, natural frequencies tend to cluster in frequency bands corresponding to the pass-bands of the structure where non-decaying waves propagate. These frequency bands are characterized by a high modal density. This was already illustrated by Zhang et al. [14] for a periodic frame structure, who used free wave propagation constants for model updating purposes; however, the influence of SSI was not yet studied.

Figure 8 shows the natural frequencies of the bridge as a function of the number of spans. The computations are performed for the case without SSI and for the stiff, medium, and soft soil. Figure 8a presents the results for the case without SSI. As the number of spans increases, the natural frequencies tend to a limit value resulting in frequency bands with different modal density. Below 5 Hz, the longitudinal translation modes of the bridge deck are found. The natural frequencies between 5 Hz and 9 Hz correspond to torsional modes, while vertical bending modes as well as torsional modes are found between 9 Hz and 12.5 Hz. Above 12.5 Hz, only torsional modes are found. For the stiff soil, the natural frequencies are shown in Figure 8b. The decrease of the natural frequencies due to the flexibility of the soil is clearly observed. The frequency band of the vertical bending modes is very narrow between 8.5 Hz and 9 Hz, approximately. Furthermore, a narrow band around 10 Hz is observed corresponding to the rotation

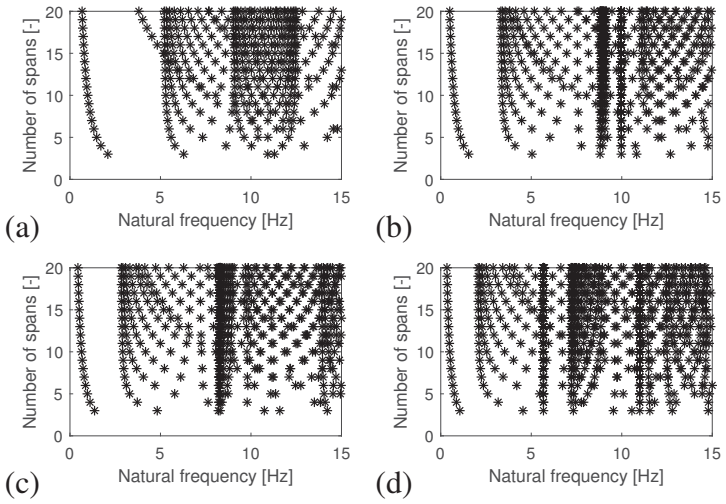

Figure 8: Natural frequencies of the bridge as a function of the number of spans computed for (a) the case without SSI, (b) the stiff soil, (c) the medium soil, and (d) the soft soil.

modes of the piers. This frequency band is also visible for the medium soil in Figure 8c around 8 Hz, nearly coinciding with the band where the vertical bending modes are situated. For the soft soil (Figure 8d), the narrow band around 5.7 Hz corresponds to the rotation modes of the piers, while the vertical bending modes are situated between 7 Hz and 9 Hz, approximately.

3.2 Dispersion curves

The dispersion curves of an infinitely long bridge in the wavenumber-frequency domain are presented in this subsection. As the bridge is periodic, the Floquet transform [15] is used to predict the forced vibration response of an infinitely long bridge due to a unit vertical eccentric load at mid-span (Figure 1a).

Figure 9 presents the vertical bridge mobility at mid-span in the wavenumber-frequency domain. Note that, in this model, the frequency dependent dynamic stiffness of the piled foundation is accounted for. The peaks observed in the forced vibration response correspond to the dispersion curves of the free waves propagating through the superstructure. These dispersion curves are obtained as the solution of an eigenvalue problem at each frequency; this originates from the condensation of the interior degrees of freedom of a reference cell and the application of Floquet theory [16, 17]. In order to reduce the computational effort, a methodology was proposed earlier [18] where advantage is taken from the fact that the bridge cross section does not vary between two piers so that the span can be subdivided in a finite number of identical cells. The dispersion curves that are superimposed on Figure 9 are: (1) the longitudinal translation mode, (2) the torsional mode, and (3) the vertical bending mode.

Figure 9a shows the dispersion curves for the case without SSI. The dispersion curves coincide with the peaks in the wavenumber-frequency domain response. The cut-on and cut-off frequencies of the dispersion curves correspond to the frequency bands observed in Figure 8a. The dispersion curve of the longitudinal translation mode does not appear as a peak in the wavenumber-frequency domain response because it is not excited by the applied load. Figure 9b shows the dispersion curves for the stiff soil. The dispersion curve of the vertical bending mode is nearly vertical, corresponding to the narrow frequency band in Figure 8b. For the medium soil, Figure 9c shows that the group velocity $\partial\omega/\partial\kappa_y$ changes sign for the vertical bending

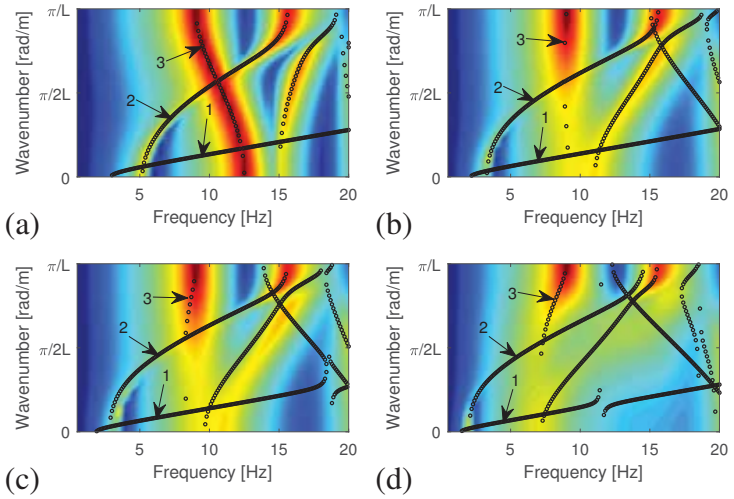

Figure 9: Logarithm of the amplitude of the vertical mobility at mid-span in the wavenumber-frequency domain. Superimposed are the dispersion curves of the non-decaying waves obtained with the WFEM: (1) the longitudinal translation mode, (2) the torsional mode, and (3) the vertical bending mode.

mode compared to the case without SSI. Figure 9d shows the dispersion curves for the soft soil. The cut-on frequency of the torsional mode equals 2 Hz, which is significantly lower than for the case without SSI (around 5 Hz). For the vertical bending mode, the cut-on frequency of the dispersion curve has decreased compared to the medium soil.

4 CONCLUSIONS

A numerical case study of a continuous concrete box girder bridge is presented in this paper. It is shown that the natural frequencies of a bridge are significantly affected by SSI when the soil is soft, particularly for the torsional modes. The influence of SSI on the mode shapes is relatively small for the lower modes, but is important for the higher modes, especially when the soil is soft. Furthermore, it has been shown that as the number of bridge spans increases, the natural frequencies converge to a limit value. These values mark the boundaries of the stop- and passbands that were observed in the dispersion curves of an infinitely long bridge. Inside the passbands, high modal density is observed. As SSI results in shift of the natural frequencies, it also affects the boundaries of the stop- and passbands of the bridge.

REFERENCES

[1] D. Feng and M.Q. Feng. Model updating of railway bridge using in situ dynamic displacement measurement under trainloads. *ASCE Journal of Bridge Engineering*, 20(12):04015019, 2015.

[2] J. Wiberg, R. Karoumi, and C. Pacoste. Optimized model updating of a railway bridge for increased accuracy in moving load simulations. In X. Perpiñà, editor, *Infrastructure Design, Signalling and Security in Railway*, chapter 8, pages 203–224. InTech, 2012.

[3] A. Romero, M. Solís, J. Domínguez, and P. Galvín. Soil-structure interaction in resonant railway bridges. *Soil Dynamics and Earthquake Engineering*, 47:108–116, 2013.

[4] J.L. Östlund, M. Ülker-Kaustell, A. Andersson, and J.-M. Battini. Considering dynamic soil-structure interaction in design of high-speed railway bridges. *Procedia Engineering*, 199:2384–2389, 2017. X International Conference on Structural Dynamics, EURODYN 2017.

[5] C. Kang, S. Schneider, M. Wenner, and S. Marx. Development of design and construction of high-speed railway bridges in germany. *Engineering Structures*, 163:184–196, 2018.

[6] B. Yan, G.-L. Dai, and N. Hu. Recent developments of design and construction of short span high-speed railway bridges in china. *Engineering Structures*, 100:707–717, 2015.

[7] J. Cascales Fernández, R. Rico Rubio, and S. Couto Wörner. Criterios de diseño sísmico en viaductos de alta velocidad en la zona de levante. *Hormigón y Acero*, 68(281):69–79, 2017.

[8] W.C. Chew and Q.H. Liu. Perfectly matched layers for elastodynamics: A new absorbing boundary condition. *Journal of Computational Acoustics*, 4(4):341–359, 1996.

[9] U. Basu and A.K. Chopra. Perfectly matched layers for time-harmonic elastodynamics of unbounded domains: theory and finite-element implementation. *Computer Methods in Applied Mechanics and Engineering*, 192(11–12):1337–1375, 2003.

[10] M. Papadopoulos, S. François, G. Degrande, and G. Lombaert. The influence of uncertain local subsoil conditions on the response of buildings to ground vibration. *Journal of Sound and Vibration*, 418:200–220, 2018.

[11] K. Miura, A.M. Kaynia, K. Masuda, E. Kitamura, and Y. Seto. Dynamic behaviour of piled foundations in homogeneous and non-homogeneous media. *Earthquake Engineering and Structural Dynamics*, 23:183–192, 1994.

[12] J.L. Östlund, A. Andersson, M. Ülker-Kaustell, and J.-M. Battini. Soil-structure interaction for foundations on high-speed railway bridges. TRITA-BKN 166, KTH Royal Institute of Technology, Stockholm, 2017.

[13] R.J. Allemang and D.L. Brown. A correlation coefficient for modal vector analysis. In *Proceedings of the 1st International Modal Analysis Conference*, pages 110–116, Orlando, Florida, 1982.

[14] J. Zhang, E. Reynders, G. De Roeck, and G. Lombaert. Model updating of periodic structures based on free wave characteristics. *Journal of Sound and Vibration*, 442:281–307, 2019.

[15] D. Clouteau, M.L. Elhabre, and D. Aubry. Periodic BEM and FEM-BEM coupling: application to seismic behavior of very long structures. *Computational Mechanics*, 25:567–577, 2000.

[16] D. Mead. Wave propagation in continuous periodic structures: research contributions from Southampton. *Journal of Sound and Vibration*, 190(3):495–524, 1996.

[17] B. Mace, D. Duhamel, M. Brennan, and L. Hinke. Finite element prediction of wave motion in structural waveguides. *The Journal of the Acoustical Society of America*, 117(5):2835–2843, 2005.

[18] P. Reumers, K. Kuo, G. Lombaert, and G. Degrande. Response of periodic elevated structures accounting for soil-structure interaction. In M. Papadrakakis and M. Fragiadakis, editors, *Proceedings of the 7th International Conference on Computational Methods in Structural Dynamics and Earthquake Engineering, COMPDYN 2019*, Crete, Greece, June 2019.